

# Voltage-Dependent Capacitors in Power Electronic Multi-Domain Simulations

U. Drofenik, A. Müsing, and J. W. Kolar

Power Electronic Systems Laboratory (PES), ETH Zurich, ETH-Zentrum / ETL H13, CH-8092 Zurich, Switzerland

**Abstract**— We discuss multi-domain simulation of power electronic systems where non-linear capacitors have a significant impact on the system behaviour, e.g. employing the MOSFET output capacitor  $C_{oss}$  for soft switching or employing nonlinear thermal models in coupled electrical-thermal simulations. It is shown which errors can result from approximating non-linear capacitors with simple linear ones as proposed e.g. for  $C_{oss}$  in datasheets. Furthermore a highly efficient implementation of non-linear capacitors in numerical circuit simulators is proposed.

**Index Terms**—Nonlinear capacitor, numerical circuit simulation, MOSFET output capacitor  $C_{oss}$ , nonlinear thermal modeling.

## I. INTRODUCTION

Numerical simulation of converter systems is essential in order to solve problems in early design stages, to speed up development, and to investigate and analyze new topologies and/or control schemes. Increasing switching speed, switching frequency, and power density, mean that more and more effects have to be accurately modeled in the simulation in order to get useful results. In this paper we discuss the use of non-linear capacitors in the power electronic circuits, and thermal modeling employing non-linear materials for coupled electrical-thermal transient simulations.

In section II of the paper we discuss fundamental equations and the definition of nonlinear capacitor, especially the nonlinear output capacitor  $C_{oss}$  of the MOSFET. We also propose a highly efficient implementation of nonlinear capacitors in numerical circuit simulation.

In section III we discuss a converter topology which employs the internal non-linear voltage-dependent capacitors  $C_{oss}$  of its power MOSFETs to achieve zero voltage switching. In this application it is essential to model and simulate the behaviour of the non-linear capacitors with high accuracy. We show that using constant capacitors in the simulation, e.g. time- or energy-related values as given in datasheets, does not work in such applications. The numerical simulations are verified by experimental measurements of the transient switching behaviour.

In Section IV the non-linear thermal behaviour of materials as typically employed in power modules and/or heat sinks is discussed. In multi-domain simulations, where transient circuit simulation is directly coupled with

thermal simulation of power semiconductor junction temperatures, the modeling of nonlinear thermal behaviour in the time-domain becomes very important in some applications, for example when highly non-linear phase change material for improving the thermal capacitance of heat sinks is employed. Reduced thermal network models have to be built using temperature-dependent thermal capacitors. The simulations employing non-linear thermal network are compared to 3D-FEM simulations.

## II. VOLTAGE-DEPENDENT CAPACITORS

### A. Definition and Measurement

The voltage-dependent capacitor's value  $C(u)$  has to be known from calculation or measurement. The according differential equation is implemented in a circuit solver. Voltage-dependent capacity  $C(u)$  can be derived from electric charge, energy, or from small-signal time behaviour. It is absolutely essential to make sure that the definition of  $C(u)$  is related to the implemented differential equation in the solver.

Equations (1) and (2) define capacity as electric charge per voltage and current as change of the electric charge. Equations (3) and (4) show that the voltage-dependent capacity  $C(u)$  based on the electric charge is different to  $C_{\Delta}(u)$  which is used in small signal calculus, see also equations (4) – (7).

$$C = \frac{q}{u} \quad (1)$$

$$i = \frac{dq}{dt} = \frac{d}{dt}(C \cdot u) \quad (2)$$

$$C = C(u) \rightarrow$$

$$i = \frac{d}{dt}(C(u) \cdot u) = \left( C(u) + u \cdot \frac{dC(u)}{du} \right) \cdot \frac{du}{dt} = C_{\Delta}(u) \cdot \frac{du}{dt} \quad (3)$$

$$C_{\Delta}(u) = C(u) + u \cdot \frac{dC(u)}{du} \quad (4)$$

$$u(t) = u_0 + \hat{u} \sin(\omega t) \quad (5)$$

$$i(t) = C_{\Delta}(u_0) \cdot \omega \cdot \hat{u} \cos(\omega t) \quad (6)$$

$$C_{\Delta}(u) = \frac{i}{du/dt} \quad (7)$$

The energy stored in a capacitor is calculated via equation (8). This allows the definition of an equivalent energy-related constant capacitor  $C_{(er)}$  which is often

given in datasheets of MOSFET output capacitors in order to calculate switching losses. This constant capacitor  $C_{(er)}$  can be calculated from the voltage-dependent small-signal capacitor  $C_{\Delta}(u)$  according to (9).

$$E_C(U) = \int_T u(t) \cdot i(t) dt = \int_T u(t) \cdot C_{\Delta}(u) \cdot \frac{du}{dt} dt = \int_U u \cdot C_{\Delta}(u) \cdot du = \frac{C_{(er)} \cdot U^2}{2} \quad (8)$$

$$C_{(er)} = \frac{2}{U^2} \cdot \int_U u \cdot C_{\Delta}(u) \cdot du \quad (9)$$

### B. Output Capacitance Coss of a MOSFET

With rising switching frequencies the correct modeling of the MOSFET output capacitor Coss in the simulation becomes more and more important. A typical voltage-dependency of Coss = Coss(u) as given in datasheets is shown in **Fig. 1**.

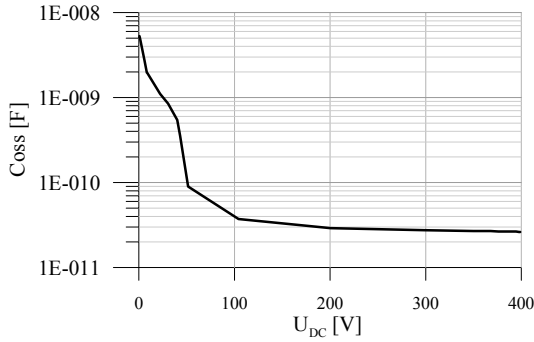


Fig. 1. Voltage-dependency of a non-linear capacitor. The characteristic shows the internal output capacity Coss(U<sub>DC</sub>) of the power MOSFET IPB60R385CP from Infineon [1].

According to [2] – [4] the output capacitor Coss(u) is based on small-signal measurement (see equations (10) and (11)). Therefore, the differential equation (12) of the non-linear capacitor has to be solved in the numerical simulation.

$$C_{oss}(u) = \frac{i}{du/dt} \quad (10)$$

$$C_{oss}(u) = C_{\Delta}(u) \quad (11)$$

$$i = C_{oss}(u) \cdot \frac{du}{dt} \quad (12)$$

### C. Efficient Implementation in a Numerical Circuit Simulator

In the numerical circuit simulation equation (12) has to be solved by the solver algorithm, for example as shown in equation (13) employing backward-Euler.

$$i = C(u) \cdot \frac{du}{dt} \rightarrow i_k = C(u^{old}) \cdot \frac{u - u^{old}}{\delta t} \quad (13)$$

Generally, performing discretization of the differential equation of each component of the electrical circuit gives the matrix equation (14) which has to be solved at each numerical time-step  $\delta t$ .

In (14) vector  $\underline{x}$  contains the node potentials of the electrical circuit (equation (15)). In general matrix  $\underline{A}$  contains the properties of the components and vector  $\underline{b}$  contains time-dependent variables like voltages ( $u^{old}$ ) and currents ( $i^{old}$ ) of the previous time-step, and values of time-dependent sources.

$$\underline{A} \cdot \underline{x} = \underline{b} \quad (14)$$

$$\underline{x} = (\varphi_1 \ \varphi_2 \ \varphi_3 \ \dots \ \varphi_n) \quad (15)$$

If the circuit elements are linear (not changing over time), matrix  $\underline{A}$  is calculated once and does not change during the simulation. Independent from component properties, vector  $\underline{b}$  has to be updated at each time-step but without calculating matrix  $\underline{A}$  at each time-step, giving a significant improvement of the simulation speed.

In power electronics circuit simulation all switches are highly non-linear components, but compared to the numerical time-step resolution, switching occurs relatively rarely. Therefore, matrix  $\underline{A}$  has to be updated every time a power switch changes state but considering the rarity of such events (compared to the many time-steps between those events) these updates have a minor effect on the simulation speed.

Matrix  $\underline{A}$  must be updated at each time-step in a straight-forward implementation with non-linear capacitors. This is obvious from equation (16) which describes the contribution from a capacitor to matrix  $\underline{A}$ .

$$\Delta a_{jk} = \pm \left( \frac{C(u^{old})}{\delta t} \right) \quad (16)$$

$$\Delta b_j = -\Delta b_k = \frac{C(u^{old})}{\delta t} \cdot (\varphi_j^{old} - \varphi_k^{old}) \quad (17)$$

In order to reduce the frequencies of the updates of matrix  $\underline{A}$ , we propose the introduction of an operating point C<sub>OP</sub> on the capacitor characteristic (10). According to (18), matrix  $\underline{A}$  is dependent on this operating point and has to be updated only when the operating point is updated. By employing C<sub>OP</sub> instead of C(u<sup>old</sup>) in matrix  $\underline{A}$ , the according entries in vector  $\underline{b}$  have to be extended by a correction factor proportional to  $i^{old}$ , the capacitor current at the previous time-step (see equation (20)). This extension guarantees the correct solution of (13) at each time-step.

$$\Delta a_{jk} = \pm \left( \frac{C_{OP}}{\delta t} \right) \quad (18)$$

$$u^{old} = \varphi_j^{old} - \varphi_k^{old} \quad (19)$$

$$\Delta b_j = -\Delta b_k = \frac{C_{OP}}{\delta t} \cdot (\varphi_j^{old} - \varphi_k^{old}) + i^{old} \cdot \left( 1 - \frac{C(u^{old})}{C_{OP}} \right) \quad (20)$$

The capacitor current is calculated from (21) at each time-step. The solver algorithm has to check at each time-step if C<sub>OP</sub> is not “too far away” from C(u), and if the current from (21) does not change its sign due to numerical effects. Otherwise, matrix  $\underline{A}$  needs no update.

$$i = \frac{C_{OP}}{\delta t} \cdot [(\varphi_j - \varphi_k) - (\varphi_j^{old} - \varphi_k^{old})] \quad (21)$$

The proposed algorithm to speed up the numerical simulation by reducing the update frequency of matrix  $\underline{A}$  significantly via operating point  $C_{OP}$  has been successfully implemented in GeckoCIRCUITS [5], a numerical simulator developed at the Power Electronic Systems Laboratory (PES), ETH Zurich. This simulator, which is optimized for power electronics, will be used for all simulations discussed below.

### III. NON-LINEAR CAPACITORS OF THE POWER SWITCH EMPLOYED IN SOFT SWITCHING STRATEGIES

#### A. Interleaved Bridgeless PFC Rectifier for High Efficiency, High Power Density Systems

**Figure 2** shows the topology of an interleaved bridgeless PFC rectifier of high efficiency and high power [6]. The converter employs the internal output capacitors  $C_{oss}$  of its power MOSFETs to achieve zero voltage switching. The currents in the individual bridge legs are in discontinuous conduction mode but add up to a sinusoidal input current due to interleaved operation.

Switching times are critical to achieve soft switching. Because of their dependency on voltage levels and load, which might change during operation, the switching times are pre-calculated via numerical simulation for all possible operating states, and available for the converter controller via look-up table [6], [7]. Therefore, it is essential to perform numerical simulations of the highest accuracy. This means, that the non-linear nature of the capacitors  $C_{oss}(u)$  has to be considered and modeled correctly.

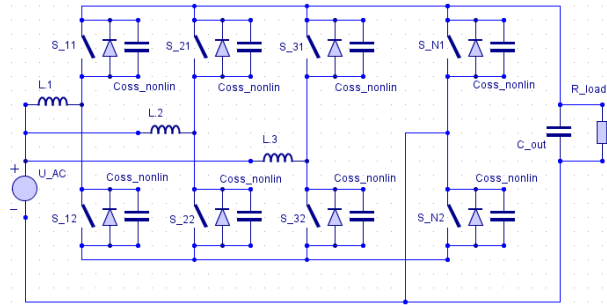


Fig. 2. Topology of interleaved bridgeless PFC rectifier employing zero voltage switching (ZVS) for high efficiency and high power density [6].

The soft switching procedure, as proposed in [6], is explained for a single boost cell of the topology in **Fig. 3**. Typical waveforms are given in **Fig. 4**.

Based on Fig. 4 we see that the current rises linearly till its maximum desired value is reached at time point (a). Switch  $S_n$  goes into off-state. Both switches are off now, and voltage  $u_{S_p}$  goes to zero while  $u_{S_n}$  rises to output voltage.  $L_{boost}$ ,  $C_p$  and  $C_n$  form the resonant circuit. Voltage  $u_{S_p}$  becomes zero at point (b). From now on zero voltage switching is possible. At point (c) we switch  $S_p$  into on-state, and the current decreases linearly. At point (d) there is enough energy stored in the inductor  $L_{boost}$  to allow sufficient resonant oscillation to achieve zero voltage switching. Voltage  $u_{S_n}$  reaches zero at point (e), and  $S_n$  can be switched loss-less into on-state

between points (e) and (g). Switching  $S_n$  after point (g) will result in undesired oscillations and prevent soft switching.

A more detailed description is shown in [6].

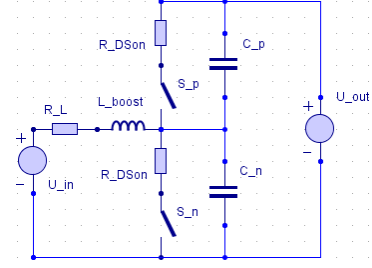


Fig. 3. Single boost cell of the topology of Fig. 2 for the positive half line cycle.

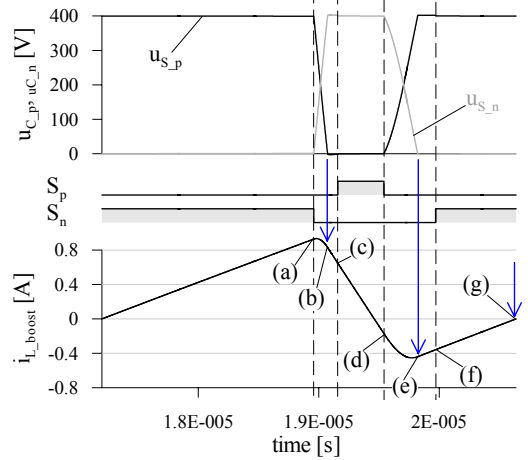


Fig. 4. Switching signals, current- and voltage-waveforms for zero voltage switching (ZVS) as proposed in [6], [7].

#### B. Effective Output Capacitance Vs. Voltage-Dependent Capacitor

As shown in the previous section, the non-linear capacitor  $C_{oss}(u)$  has a significant impact on the converter operation. One might consider employing a linear (constant) equivalent capacitor instead, for simplification purposes, which would result in comparable (time) behaviour. In the following we will discuss such an approach and show that equivalent capacitor values as proposed in datasheets often do not give useful results.

For calculation or estimation of switching losses related to  $C_{oss}$ , datasheets often give an equivalent energy-related value labeled e.g. as  $C_{o(er)}$ . This capacitance  $C_{o(er)}$  is defined as fixed capacitance that gives the same stored energy as  $C_{oss}$  while  $V_{DS}$  is rising from 0 to 80% (definition from [1]). As one can see from equation (9), this value is not related e.g. to a  $C_{oss}$ -value on the characteristic (10). Employing  $C_{o(er)}$  in a numerical simulation of the soft switching procedure results in the waveforms shown in **Fig. 5**. According to its definition,  $C_{o(er)}$  is not intended for simulations of waveforms in the time-domain. The resulting waveforms are therefore, not surprisingly, quite different from the correct waveforms where  $C_{oss}$  is correctly modeled as voltage-dependent capacitor.

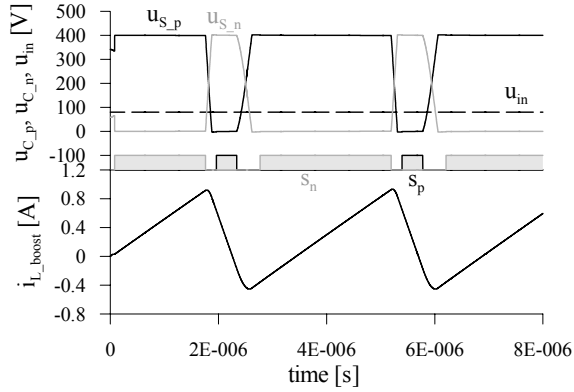


Fig. 5. Transient simulation of the switching behaviour of the topology shown in Fig. 2 employing a constant energy-related MOSFET output capacitor  $C_{oss} = C_{o(er)} = 130\text{pF}$ .

In some datasheets an equivalent time-related value for a linear (constant) capacitor is given. According to e.g. [1] the value of this equivalent capacitor  $C_{o(tr)}$  is defined as fixed capacitance that gives the same charging time as  $C_{oss}$  while  $V_{DS}$  is rising from 0 to 80%. Employing this capacitor  $C_{o(tr)}$  in a transient simulation results in the curves given in Fig. 6. Although this capacitance  $C_{o(tr)}$  is related to the time-domain, the waveforms are significantly different to the simulation employing a non-linear capacitor  $C_{oss}(u)$  as shown in the following.

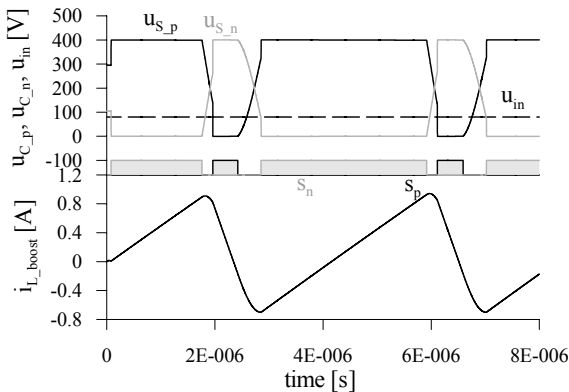


Fig. 6. Transient simulation of the switching behaviour of the topology shown in Fig. 2 employing a constant time-related MOSFET output capacitor  $C_{oss} = C_{o(tr)} = 340\text{pF}$ .

Implementing the algorithm proposed in section II in the power electronic circuit simulator GeckoCIRCUITS [5],  $C_{oss}$  is modeled as non-linear voltage-dependent capacitor  $C_{oss}(u)$  as given in Fig. 1 and/or [1]. Resulting waveforms for the soft switching procedure are shown in Fig. 7. The simulated currents of Fig. 5, 6 and 7 are compared in Fig. 8. One can clearly see the error resulting from employing equivalent linear (constant) capacitors.

If times for the soft switching procedure are taken from look-up tables based on numerical simulations, as discussed at the beginning of section III and/or in [6], [7], one must obviously employ non-linear capacitor models in the simulation in order to guarantee reliable zero voltage switching during operation of the converter hardware.

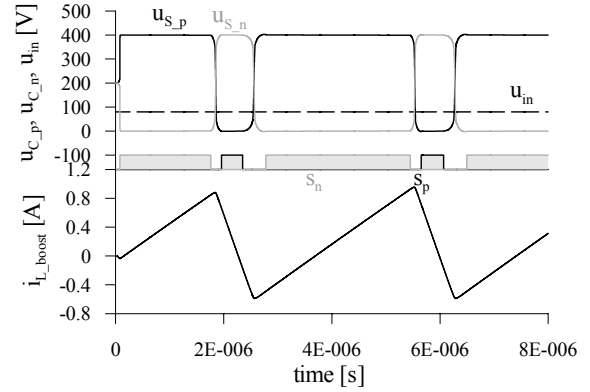


Fig. 7. Transient simulation of the switching behaviour of the topology shown in Fig. 2 employing a nonlinear voltage-dependent MOSFET output capacitor  $C_{oss} = C_{oss}(u)$ .

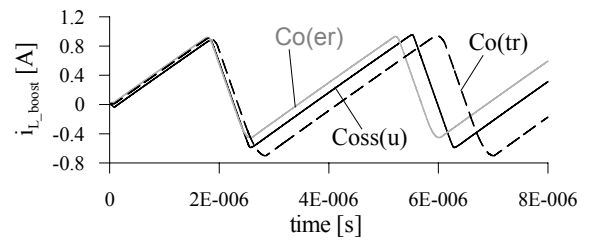


Fig. 8. Comparison of the three transient simulations in Fig. 5, 6, and 7 with different models for the MOSFET output capacitor  $C_{oss}$ : constant energy-related capacitor  $C_{o(er)}$ , constant time-related capacitor  $C_{o(tr)}$ , and nonlinear voltage-dependent capacitor  $C_{oss}(u)$ .

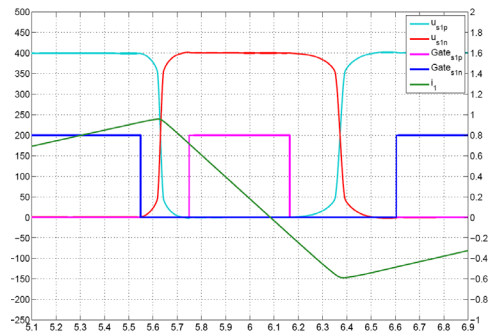


Fig. 9. Circuit model in GeckoCIRCUITS [5] employing nonlinear voltage-dependent MOSFET output capacitors  $C_{oss}(u)$ . Simulation of switching signals, current- and voltage-waveforms for zero voltage switching (ZVS) [7].

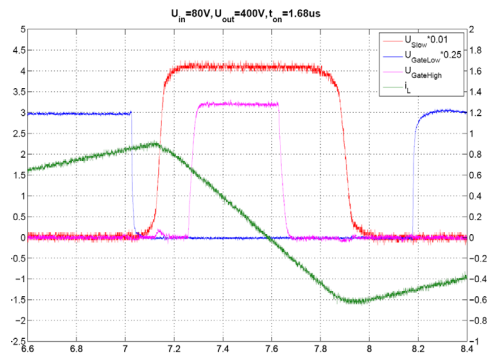


Fig. 10. Experimental measurements [7] of switching signals, current- and voltage-waveforms for zero voltage switching (ZVS).

### C. Experimental Verification

In order to verify the soft switching procedure proposed in [6] and the correct implementation of the non-linear capacitor in GeckoCIRCUITS, experimental measurements of the waveforms during zero-voltage switching have been performed at different operating states. Comparing the numerical simulation (**Fig. 9**) with the measurement e.g. at  $U_{in} = 80V$ ,  $U_{out} = 400V$  and  $t_{on} = 1.68\mu s$  (**Fig. 10**), one can see a very good agreement [7].

## IV. NON-LINEAR CAPACITORS IN POWER ELECTRONICS MULTI DOMAIN SIMULATIONS

### A. Thermal Modeling of Power Module Materials

A typical example for a multi-domain simulation is the transient calculation of the junction temperature of a power switch during converter operation. The losses of the switch are temperature dependent which has an impact on the converter efficiency and its electrical behaviour, and the electrical behaviour influences the semiconductor losses.

In order to include the thermal domain in the numerical simulation and couple it with the electrical model, a reduced thermal model has to be built. If this was not done, the simulation times would be too long in many applications.

One can divide a three-dimensional structure, such as a power module on a heat sink, into many small volume cells. In a second step, the heat conduction equation (22) is linearized within each cell volume. This is equivalent to a node in the cell center with a thermal capacity to ground (ambient temperature) and with thermal resistors for heat conduction through the cell. Such a cell is shown in **Fig. 11**. The values for  $R_{th}$  and  $C_{th}$  come directly from equation (22). This method is known as Finite Difference Method (FDM).

$$\rho \cdot C_p(T) \cdot \frac{\partial T}{\partial t} = \nabla \cdot (k(T) \nabla T) + \dot{W}(\vec{x}, t) \quad (22)$$

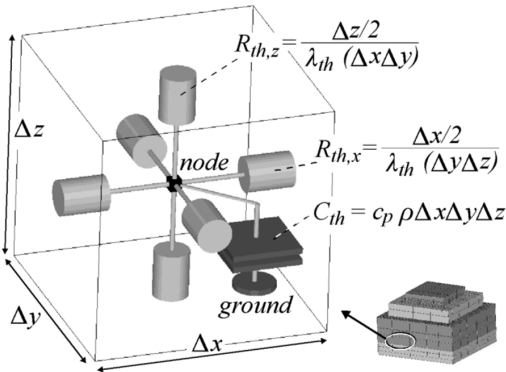


Fig. 11. Three-dimensional thermal equivalent circuit of a small three-dimensional volume cell [8].

Use of the FDM makes it possible to calculate the temperature field within the whole structure if a large number of small enough cells is employed. A large cell number gives large calculation effort. Therefore, coupling

such a thermal model with a transient circuit simulation will give extremely long simulation times. Typically, one is mainly interested in transient temperature at a very small number of geometric points, for example the junction temperature.

In this case a compact thermal model can be created. The cell number is reduced significantly in a way that only the temperature at a single geometric point of interest is defined correctly. This is called a Cauer network and is shown in **Fig. 12(a)**. Note that the nodes are still connected by thermal resistors and grounded by thermal capacitors, just as shown in Fig. 11.

As an alternative a Foster network (**Fig. 12(b)**) can be used. The idea here is to parameterize  $R_{th}$  and  $C_{th}$  in a way that the network input node behaves exactly as the junction. Parameterization is performed via mathematical fitting of thermal step responses, and is not related to physics.

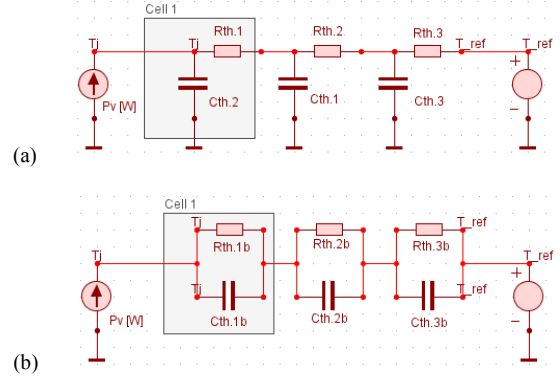


Fig. 12. Thermal equivalent circuits for embedding thermal models in transient power electronics simulation: (a) Cauer network, (b) Foster network.

The basis of all this modeling theory is the assumption that the heat conduction equation (22) is linear which means that the thermal material properties are not temperature dependent.

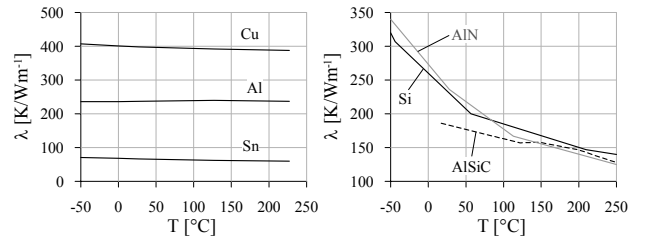


Fig. 13. Temperature dependency of the thermal conductivity of selected materials used in power modules [9].

**Figure 13** shows the temperature dependency of thermal conductivity for a few typical materials employed in power modules and heat sinks. Metals are not sensitive in typical power electronics temperature ranges, but materials like ceramic or *Si* are clearly temperature dependent. It is shown in [9] that ignoring this temperature dependency in typical operating temperatures ranges results in errors below 5%.

In case of wider temperature ranges (application dependent) or different temperature levels (e.g.

employing *SiC*) is desirable to take such non-linearity into account via temperature-dependent resistors.

In the following we discuss temperature dependency of the thermal capacity which can be modeled by a non-linear capacitor  $C_{th}(T)$  with the same mathematical properties as the electrical capacitor  $C(u)$  described in section II.

According to [10] the temperature-dependency of solid materials is (partly) defined by equations (23) and (24) with  $N$  and  $k$  as material properties, and the characteristic Debye temperature  $T_D$  of a material. The equations (23) and (24) give the curve in **Fig. 14**, see also [10]. Properties of materials typically employed in power electronics are given in **Table I**.

$$T \ll T_D \dots \frac{C_V}{Nk} \sim \left(\frac{T}{T_D}\right)^3 \quad (23)$$

$$T \gg T_D \dots \frac{C_V}{Nk} \sim const \quad (24)$$

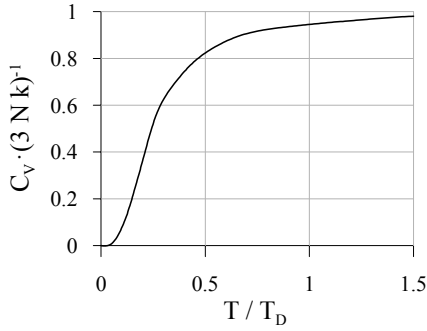


Fig. 14. Debye model for predicting temperature dependent thermal heat capacity [10].

As long as the operating temperature range is close to or larger than the Debye temperature  $T_D$ , the heat capacity of a material can be modeled in good approximation with a linear (constant) capacitor. Ceramic materials such as *AlN* or *Al<sub>2</sub>O<sub>3</sub>*, exhibit the ratio  $T/T_D$  is 0.37 at 100°C. At this point the slope in Fig. 14 is steep indicating a strong temperature-dependence. For metal *Al* (*Cu*) the ratio at 100°C is 0.87 (1.08) where the small slope indicates negligible temperature-dependency.

TABLE I

PROPERTIES RELATED TO TEMPERATURE-DEPENDENT HEAT CAPACITY OF SELECTED MATERIALS [11]

	Ceramic ( <i>AlN</i> , <i>Al<sub>2</sub>O<sub>3</sub></i> )	Si	Al	Cu
$c_p$ [J/kgK] for $T < 77K$	61	180	336	195
$c_p$ [J/kgK] for $T > 373K$	910	770	937	397
density [kg/m <sup>3</sup> ]	3970	2330	2800	2700
$T_D$ [K]	1150 ( <i>AlN</i> ) 980 ( <i>Al<sub>2</sub>O<sub>3</sub></i> )	645	428	344

In special temperature environments and/or future applications (e.g. employing *SiC*) it might become important to model non-linear thermal capacitors. If the thermal capacitance  $C_P(T)$  is available e.g. from small signal measurement, a simulator has to implement equation (13) with temperature replacing voltage and heat flow replacing electrical current.

## B. Thermal Management Employing Highly Nonlinear Materials Like Phase Change Materials

A typical heat sink consists of a base plate and fins. The base plate has to smooth hot spots and guide the heat flow to the fins. The fins dissipate the heat via convection into the air flow channel. Base plate and fins contribute to the thermal capacity of the heat sink.

If a converter operates under load cycles (e.g. a train going to a station, stopping there, and continuing to the next station; or an electric car in stop-and-go mode; or a mechanical actuator operating during short periods compared to long intervals of inactivity) the semiconductor temperatures will cycle between high and low operating temperatures. This weakens solder connections in power modules due to a thermal mismatch which results in reduced lifetime.

In [12] it is proposed to smooth thermal cycles and/or reduce temperature peaks by increasing the heat sink's thermal capacity by adding or inserting phase change material. Reduced peaks and/or cycle amplitudes will improve lifetime and reliability of the system.

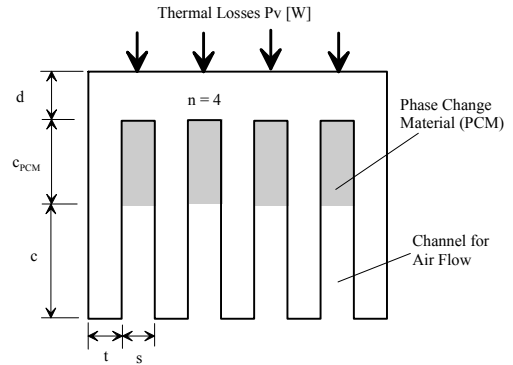


Fig. 15. Heat sink with integrated phase change material to increase thermal capacity. Forced convection creates air flow in the channels.

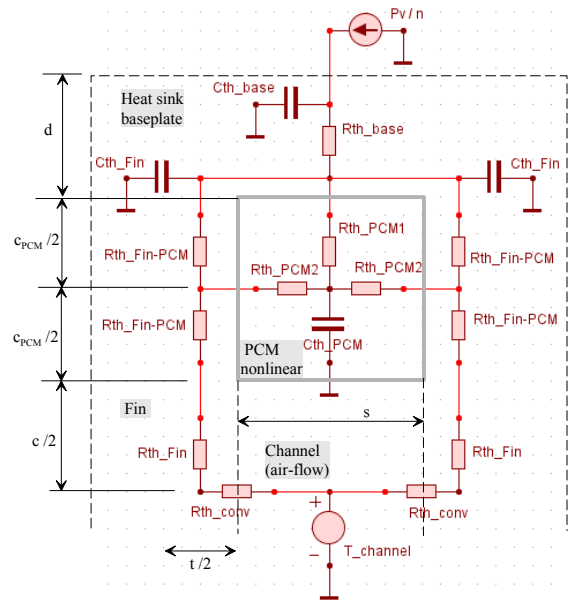


Fig. 16. Thermal network model of the heat sink (Fig. 15) employing phase change material and convection cooling by forced airflow through a channel. The model shows two half-fins (vertical cross section) and the PCM-filled space in between. [12]

**Figure 15** shows a typical heat sink with phase change material (PCM) embedded where the fins are connected to the base plate. A simple but accurate thermal network model of the structure of Fig. 15 is given in **Fig. 16** (see [12] for details). The PCM in the space between two fins is modeled as one thermal cell (Fig. 11) with a thermal capacitor  $C_{th\_PCM}$  in the center node.

According to [13] - [15] the thermal behaviour of the PCM can be described by differential equations (25) and (26) where  $\Delta H$  [kJ/kg] is the latent heat of melting which is a material property specifying the heat absorbed during the change of phase. The temperature range, over which the PCM melts, is given by  $\Delta T$  in (26).

$$\rho C(T) \cdot \frac{\partial T}{\partial t} = \nabla \cdot (k \nabla T) \quad (25)$$

$$C(T) = C_p + \frac{\Delta H}{\Delta T} \quad (26)$$

The temperature-dependent thermal capacity of PCM is given according to [13] in equation (27). The shape of this characteristic is quite different from e.g.  $C_{oss}(u)$  in Fig. 1 or from the thermal capacities in Fig. 14.  $C(T)$  in (27) is constant with a rectangular-shaped peak around the melting temperature. It becomes obvious from the definitions (25) - (27) that the thermal equivalent of equation (13) must be employed for the implementation of equation (25) in the solver with  $C(T)$  as given in (27).

$$C(T) = \begin{cases} C_p & \text{for } T < T_{melt} \\ C_p + \frac{\Delta H}{\Delta T} & \text{for } T_{melt} < T < T_{melt} + \Delta T \\ C_p & \text{for } T_{melt} + \Delta T < T \end{cases} \quad (27)$$

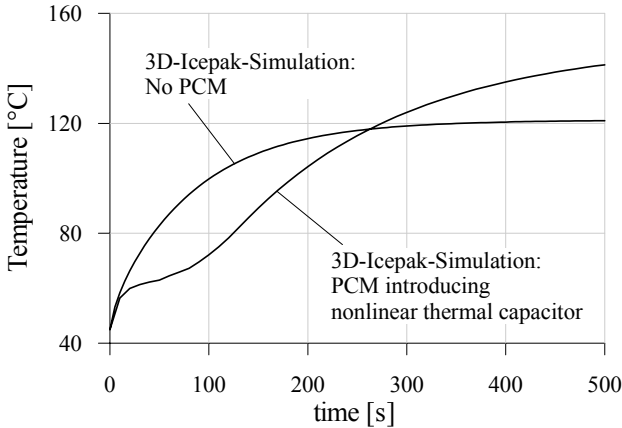


Fig. 17. Simulation of a temperature step response employing the fluid dynamics solver Icepak (three-dimensional FEM simulation) with and without phase change material embedded in the heat sink. [12]

**Figure 17** shows a transient simulation of a step response of a heat sink with and without phase change material. Both simulations are performed with the three-dimensional fluid dynamics solver Icepak [11] which is based on the Finite Element Method (FEM). The PCM is modeled as material with a non-linear capacitance according to the definition in equation (27).

The same transient simulation is performed using the simple network model of Fig. 16 in GeckoCIRCUITS where non-linear thermal networks can be built for electrical-thermal coupling. The results shown in **Fig. 18** are in very good agreement to the simulations in Fig. 17. The main difference to the Icepak simulation in Fig. 17 is that Icepak calculates thousands of thermal cells for a three-dimensional geometry and can, therefore, describe the time- and space-depending melting process with much higher accuracy.

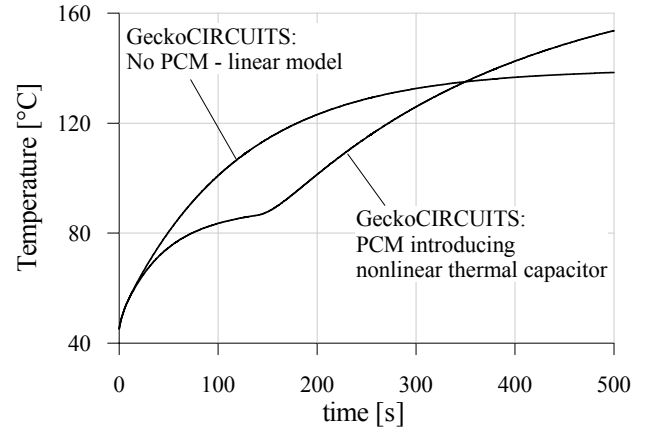


Fig. 18. Simulation of a temperature step response employing circuit simulator GeckoCIRCUITS with and without phase change material embedded in the heat sink. The thermal network of Fig. 16 is employed, and the capacitor  $C_{th\_PCM}$  is modeled according to equation (27) as nonlinear temperature-dependent device. [12]

As shown in Fig. 17 and Fig. 18, it is possible to temporarily reduce temperature in a certain time range by employing PCM. This works well for load pulses of defined duration. Due to the relatively high thermal resistance of PCMs, stationary temperatures might be significantly increased, which provides limits for this approach.

## V. CONCLUSIONS

It is critical to exactly know the definition and measurement method of a non-linear capacitance characteristic  $C(u)$  when building a model for a numerical simulation. If  $C(u)$  is based on small-signal measurement, it can be directly employed in GeckoCIRCUITS, an optimized power electronics simulator developed at the Power Electronic Systems Laboratory (PES), ETH Zurich.

It is shown for a PFC rectifier topology which employs the MOSFETs' internal capacitors  $C_{oss}$  for zero voltage switching, that it is very important to perform transient simulations considering the voltage dependency of  $C_{oss} = C_{oss}(u)$ . Employing equivalent linear capacitances, e.g. energy-related  $C_{o(er)}$  or time-related  $C_{o(tr)}$ , as given in datasheets, can result in significant errors. The simulations in the time-domain are experimentally verified.

In certain power electronic problems (electrical-thermal coupling) it is important to accurately model the temperature-dependency of the thermal capacitance in order to build reliable thermal models. It is shown that

such modeling can be done easily based on the non-linear capacitor implementation discussed in section II of the paper. As example, a heat sink with embedded highly non-linear phase change material is simulated and verified by a 3D-FEM simulation.

## APPENDIX

### A. Non-Linear Current-Dependent Inductive Components

Although not a topic of this paper, it should be mentioned that the non-linear inductive component, which is common in power electronics, e.g. a saturating inductor, follows similar definitions as the capacitor discussed in section II.

Generally, inductance can be related to magnetic flux per current, stored magnetic energy, small-signal measurement of voltage and current, or the B(H) characteristic of magnetic material. It is essential to understand the exact definition (and/or measurement method) of the non-linear inductor  $L(i)$  before setting up a simulation model.

Equations (A.1) – (A.7) show the relationship between non-linear inductance  $L(i)$  defined via magnetic flux compared to the small-signal  $L_{\Delta}(i)$ , see equation (A.7). The stored energy calculated via equation (A.8) allows defining an energy-related linear (constant) inductance  $L_{(er)}$  as given in (A.9).

$$L = \frac{\psi}{i} \quad (A1)$$

$$u = \frac{d\psi}{dt} = \frac{d}{dt}(L \cdot i) \quad (A2)$$

$$L = L(i) \rightarrow$$

$$u = \frac{d}{dt}(L(i) \cdot i) = \left( L(i) + i \cdot \frac{dL(i)}{di} \right) \cdot \frac{di}{dt} = L_{\Delta}(i) \cdot \frac{di}{dt} \quad (A3)$$

$$L_{\Delta}(i) = L(i) + i \cdot \frac{dL(i)}{di} \quad (A4)$$

$$i(t) = i_0 + \hat{i} \sin(\omega t) \quad (A5)$$

$$u(t) = L_{\Delta}(i_0) \cdot \omega \cdot \hat{i} \cos(\omega t) \quad (A6)$$

$$L_{\Delta}(i) = \frac{u}{di/dt} \quad (A7)$$

$$E_L(I) = \int_T u(t) \cdot i(t) dt = \int_T L_{\Delta}(i) \cdot \frac{di}{dt} \cdot i(t) dt =$$

$$= \int_I u \cdot L_{\Delta}(i) \cdot di = \frac{L_{(er)} \cdot I^2}{2} \quad (A8)$$

$$L_{(er)} = \frac{2}{I^2} \cdot \int_I i \cdot L_{\Delta}(i) \cdot di \quad (A9)$$

The differential equation of the non-linear small-signal inductor  $L_{\Delta}(i)$  is implemented in GeckoCIRCUITS. This

means that a small-signal measurement of an inductance can be directly employed in this circuit simulator. The non-linear inductor in GeckoCIRCUITS was successfully modeled, tested and experimentally verified for application in audio amplifiers in [16].

## REFERENCES

- [1] Infineon, datasheet of MOSFET IPB60R385CP
- [2] International Rectifier, "A More Realistic Characterization of Power MOSFET Output Capacitance Coss", Application Note AN-1001
- [3] Infineon, "Explanation of Data Sheet Parameters", Explanation, V 1.0, April 2002
- [4] A. Karvonen, T. Thiringer, "MOSFET Modeling Adapted for Switched Applications Using a State-Space Approach and Internal Capacitance Characterization", Proceedings of the 8th International Conference on Power Electronics and Drive Systems (PEDS'09), Taipei, Taiwan, Nov. 2 -5, 2009.
- [5] GeckoCIRCUITS, online version at [www.gecko-research.com](http://www.gecko-research.com)
- [6] C. Marxgut, J. Biela, J. W. Kolar, "Novel Interleaved Bridgeless PFC Rectifier Topology for High Efficiency, High Power Density Systems", International Power Electronics Conference- ECCE Asia - IPEC-Sapporo 2010, Sapporo, Japan, June 21 - 24, 2010.
- [7] C. Beck, "Auslegung und Aufbau eines Ultraflachen Gleichrichters", master thesis at PES/ETH Zurich, Switzerland, March 2010.
- [8] U. Drogenik, "Embedding Thermal Modeling in Power Electronic Circuit Simulation", Proceedings of the ECPE Power Electronics Packaging Seminar (PEPS'04), Baden-Dättwil, Switzerland, June 7 - 8, 2004.
- [9] U. Drogenik, D. Cottet, A. Müsing, J.-M. Meyer, J. W. Kolar, "Modelling the Thermal Coupling between Internal Power Semiconductor Dies of a Water-Cooled 3300V/1200A HiPak IGBT Module", Proceedings of the Conference for Power Electronics, Intelligent Motion, Power Quality, Nuremberg, Germany, May 22 - 24, 2007.
- [10] M. Razeghi, "Fundamentals of Solid State Engineering", ISBN-13: 978-0387281520, Springer, Berlin, 2006.
- [11] Fluid-dynamics simulation software Icepak at [www.icepak.com](http://www.icepak.com)
- [12] A. Stupar, U. Drogenik, J. W. Kolar, "Application of Phase Change Materials for Low Duty Cycle High Peak Load Power Supplies", Proceedings of the 6th International Conference on Integrated Power Electronic Systems (CIPS 2010), Nuremberg, Germany, March 16 - 18, 2010.
- [13] E. M. Alawadhi, C. Amon, "PCM Thermal Control Unit for Portable Electronic Devices: Experimental and Numerical Studies", IEEE Transactions on Components and Packaging Technologies, Vol. 26, No. 1, March 2003.
- [14] S. Krishnan, S. V. Garimella, S. S. Kang, "A Novel Hybrid Heat Sink using Phase Change Materials for Transient Thermal Management of Electronics", IEEE Transactions on Components and Packaging Technologies, Vol. 28, No. 2, June 2005.
- [15] N. Zheng, R. A. Wirtz, "A Hybrid Thermal Energy Storage Device, Part 1: Design Methodology", ASME Journal of Electronic Packaging, Vol. 126, March 2004.
- [16] A. Knott, T. Stegenborg-Andersen, O. C. Thomsen, D. Bortis, J. W. Kolar, G. Pfaffinger, M. A. E. Andersen, "Modeling Distortion Effects in Class-D Amplifier Filter Inductors", Proc. of the 128th Convention of the Audio Engineering Society, London, UK, May 22 - 25, 2010.